Atmos. Chem. Phys. Discuss., doi:10.5194/acp-2017-219, 2017
Manuscript under review for journal Atmos. Chem. Phys.
Discussion started: 19 April 2017

Atmospheric Chemistry and Physics Discussions

A HIGH-RESOLUTION AND OBSERVATIONALLY CONSTRAINED OMI NO_2 SATELLITE RETRIEVAL

Daniel L. Goldberg*[1,2], Lok N. Lamsal [3,4], Christopher P. Loughner [5,6], Zifeng Lu [1,2], and David G. Streets [1,2]

[1]Energy Systems Division, Argonne National Laboratory, Argonne, IL 60439, USA

[2]Computation Institute, University of Chicago, Chicago, IL 60637, USA

[3]Goddard Earth Sciences Technology and Research, Universities Space Research Association, Columbia, MD 21046, USA

[4]NASA Goddard Space Flight Center, Code 614, Greenbelt, MD 20771, USA

[5]NOAA Air Resources Laboratory, College Park, MD 20740, USA

[6]Earth System Science Interdisciplinary Center, University of Maryland, College Park, MD 20740, USA

*Corresponding author. Phone: (630) 252-3931; Fax: (630) 252-8007; Email: dgoldberg@anl.gov.

Atmos. Chem. Phys. Discuss., doi:10.5194/acp-2017-219, 2017
Manuscript under review for journal Atmos. Chem. Phys.
Discussion started: 19 April 2017

Atmospheric Chemistry and Physics Discussions

A high-resolution and observationally constrained OMI NO_2 satellite retrieval

Daniel L. Goldberg[1,2], Lok N. Lamsal[3,4], Christopher P. Loughner[5,6], Zifeng Lu[1,2], and David G. Streets[1,2]

[1]Energy Systems Division, Argonne National Laboratory, Argonne, IL 60439, USA
[2]Computation Institute, University of Chicago, Chicago, IL 60637, USA
[3]Goddard Earth Sciences Technology and Research, Universities Space Research Association, Columbia, MD 21046, USA
[4]NASA Goddard Space Flight Center, Code 614, Greenbelt, MD 20771, USA
[5]NOAA Air Resources Laboratory, College Park, MD 20740, USA
[6]Earth System Science Interdisciplinary Center, University of Maryland, College Park, MD 20740, USA

Correspondence to: Daniel L. Goldberg (dgoldberg@anl.gov)

Abstract. This work presents a new high resolution NO_2 dataset derived from the standard NASA Ozone Monitoring Instrument (OMI) NO_2 version 3.0 retrieval that can be used to estimate surface level concentrations. The standard NASA product uses NO_2 vertical profile shape factors from a 1.25° × 1° (~110 × 110 km) resolution Global Model Initiative (GMI) model simulation to calculate air mass factors, a critical value used to determine observed tropospheric NO_2 vertical columns. To better estimate vertical profile shape factors, we use a high resolution Community Multi-scale Air Quality (CMAQ) model simulation (1.33 × 1.33 km) to generate tropospheric air mass factors and tropospheric NO_2 columns during summertime in the eastern United States. Results show OMI NO_2 tropospheric columns in this new product increase by up to 160 % in city centers, and decrease by 20 – 50 % in the rural areas outside of urban areas when compared to the operational product. This new product shows much better agreement with the Pandora NO_2 spectrometer measurements acquired during the DISCOVER-AQ Maryland field campaign. Furthermore, the correlation between this satellite product and EPA NO_2 monitors in urban areas has improved dramatically: r^2 = 0.60 in new product, r^2 = 0.39 in operational product, signifying that this new product is a better indicator of surface concentrations than the operational product. Our work emphasizes the need to use high resolution models to re-calculate satellite data in areas with large spatial heterogeneities in NOx emissions. Although the current work is focused on the eastern United States, the methodology developed in this work can be applied to other world regions to produce high-quality region-specific NO_2 satellite retrievals.

Atmos. Chem. Phys. Discuss., doi:10.5194/acp-2017-219, 2017
Manuscript under review for journal Atmos. Chem. Phys.
Discussion started: 19 April 2017

Atmospheric Chemistry and Physics Discussions

1 Introduction

Tropospheric NO_2 is a trace gas toxic to human health and during ideal atmospheric conditions can photolyze to create O_3 another toxic air pollutant with a longer atmospheric lifetime. The eventual fate of tropospheric NO_2 is often HNO_3, a chemical species easily dissolved in water and responsible for acid rain. HNO_3 can also react with ammonia to create nitrate aerosols, which contribute to haze and are harmful to human health.

There are some natural sources of nitrogen oxides ($NO_x \equiv NO+NO_2$), such as from soil through microbial nitrification and denitrification (Conrad, 1996), lightning (Ridley et al., 1996), and natural wildfires (Val Martin et al., 2006), but the majority of the NO_2 in our atmosphere today originates from anthropogenic sources (van Vuuren et al., 2011). When temperatures are greater than 1500 K, such as in fuel combustion, nitrogen (N_2) and oxygen (O_2) spontaneously react to create NO via the endothermic Zeldovich mechanism. The nitrogen in fuels are also converted to NO during combustion making fuels rich in nitrogen, such as coal, more efficient at creating NO. NO is quickly oxidized to NO_2 in the atmosphere, most often by ozone, in a matter of seconds. Thus the NO and NO_2 species are often grouped into a single species called NO_x. In the presence of HO_2, NO can also be oxidized to NO_2 without consuming ozone. This is the rate-limiting step in the chemical chain reaction producing tropospheric ozone.

NO_2 is a strong absorber of radiation within the 400 – 450 nm wavelength region (Vandaele et al., 1998), which approximately corresponds to violet visible light. Satellite instruments measure the absorption of solar backscatter in the UV-visible spectral range, enabling estimation of the amount of NO_2 in the atmosphere between the instrument and the surface. By comparing observed spectra with a reference spectrum, we can derive total column amounts; this technique is called differential optical absorption spectroscopy (DOAS) (Platt, 1994).

NO_2 has been continuously measured from satellites for over two decades now. The first instrument to remotely measure NO_2 was the Global Ozone Monitoring Experiment (GOME) launched aboard the ERS-2 satellite in April 1995 (Burrows et al., 1999). Despite its coarse temporal and spatial resolution (global coverage once every three days and pixel size of 40 × 320 km), it was the first remotely sensed instrument to characterize NO_2 columns from space, showing enhanced tropospheric NO_2 over North America and Europe (Martin et al., 2002; Martin et al., 2003). In the early 2000s, Scanning Imaging Absorption Spectrometer for Atmospheric Chartography (SCIAMACHY) (Bovensmann et al., 1999) and Ozone Monitoring Instrument (OMI) (Levelt et al., 2006; Bucsela at el., 2006; Boersma et al., 2007) became additional space-based instruments to measure NO_2. These instruments were designed to achieve better spatial resolution (SCIAMACHY: 30 × 60 km, OMI: 13 × 24 km) than GOME. Boersma et al. (2008a) documented the differences between the two retrievals. In early 2012, ground operators lost contact with SCIAMACHY, but OMI is still operational as of 2017. There are two operational OMI NO_2 retrievals: the KNMI DOMINO v2.0 product (Boersma et al., 2007) and the NASA OMNO2 v3.0 product (Krotkov et al., 2017).

Atmos. Chem. Phys. Discuss., doi:10.5194/acp-2017-219, 2017
Manuscript under review for journal Atmos. Chem. Phys.
Discussion started: 19 April 2017

Atmospheric Chemistry and Physics Discussions

OMI NO_2 has been used to estimate NO_x emissions from various areas around the globe (Streets et al., 2013) including North America (Boersma et al., 2008b; Lu et al., 2015), Asia (Zhang et al., 2008; Han et al, 2015; Kuhlmann et al., 2015), the Middle East (Beirle et al., 2011), and Europe (Huijnen et al., 2010; Curier et al., 2014). It has also been used to generate and validate NO_x emission estimates from source sectors such as soil (Hudman et al., 2010; Vinken et al., 2014a; Rasool et al., 2016), lightning (Allen et al., 2012; Liaskos et al., 2015; Pickering et al., 2016), power plants (de Foy et al., 2015), aircraft (Pujadas et al., 2011), marine vessels (Vinken et al., 2014b; Boersma et al., 2015), and urban centers (Lu et al., 2015; Canty et al., 2015; Souri et al., 2016). More recently, there has been an emphasis on analyzing emission trends because OMI has been retrieving high-quality tropospheric NO_2 data for over ten years. Over this decade, some areas have seen increases, such as India (Lu and Streets, 2012), China (Verstraeten et al., 2015), the Canadian oil sands region (McLinden et al., 2015), and other oil extraction regions (Duncan et al., 2016), while areas such as the eastern United States (Russell et al., 2012; Lamsal et al., 2015; Krotkov et al., 2016) and Europe (Curier et al., 2014; Duncan et al., 2016) have seen large decreases due to a switch to cleaner fuels and the implementation of emission control technologies.

One of the reasons why the usage of satellite data remains tepid in policy-making communities is due to their inability to detect surface concentrations; improving this ability may spur their use. In particular, detecting the spatial heterogeneities of NO_2 in and around city centers are of strong interest as many people are exposed to NO_2 or co-located pollutants exceeding policy thresholds in these areas. Satellite measurements with spatial resolution > 13 km, such as OMI, have difficulty observing the fine structure of NO_2 plumes at or near the surface (e.g., highways, power plants, factories, etc.) (Chen et al., 2009; Ma et al., 2013; Flynn et al., 2014), which are often less than 10 km in width (Heue et al., 2008). This can lead to a spatial smoothing of pollution, which does not exist in reality (Hilboll et al., 2013). Remote sensing instruments with finer spatial resolution, such as TROPOMI (Veefkind et al., 2012) and TEMPO (Zoogman et al., 2017), may be able to resolve this issue.

Until the next generation of satellites is launched, there have been several techniques to modify OMI NO_2 data a posteriori. Kim et al. (2016) developed a technique in which users can utilize regional air quality model information to spatially downscale OMI NO_2 measurements. This technique has shown to increase the variability of OMI NO_2 within urban areas, which is in better agreement with observations in these regions. In another effort to merge model and satellite data, Lamsal et al. (2008) was able to infer surface level NO_2 concentrations from OMI NO_2 by applying local scaling factors from a global model. There has also been an emergence of a technique that combines land-use regression techniques with satellite information to infer ground-level NO_2 concentrations (Novotny et al., 2011; Vienneau et al., 2013; Lee et al., 2014; Bechle et al., 2015; Young et al., 2016). While each individual technique is useful, all of the aforementioned techniques use model data to adjust existing satellite data, but do not address issues inherent with the satellite retrieval methodology.

2 Methods

We use a method to re-calculate satellite data in lieu of using the operational product as is. There are three existing NO_2 products that follow a similar procedure: BeHR for the United States (Russell et al., 2011; Laughner et al.,

Atmos. Chem. Phys. Discuss., doi:10.5194/acp-2017-219, 2017
Manuscript under review for journal Atmos. Chem. Phys.
Discussion started: 19 April 2017

Atmospheric Chemistry and Physics Discussions

2016), POMINO for China (Lin et al., 2015), and HKOMI for the Pearl River Delta region of China (Kuhlmann et al., 2015). We build upon these studies by using an even higher resolution regional air quality model (1.33 km) to generate air mass factors, a value needed for calculation of tropospheric vertical column NO_2 amounts. We use a small region in the eastern United States as a case study in developing high resolution NO_2 tropospheric columns for urban metropolitan areas (200 × 200 km).

2.1 OMI NO_2

The Ozone Monitoring Instrument (OMI) has been operational on NASA's Earth Observing System (EOS) Aura satellite since October 2004 (Levelt et al., 2006). The satellite follows a sun-synchronous, low-earth (705 km) orbit with an equator overpass time of approximately 13:45 local time. OMI measures total column amounts in a 2600 km swath divided into 60 unequal area "field-of-views", or pixels. At nadir (center of the swath), pixel size is 13 × 24 km, but at the swath edges, pixels can be as large as 26 × 128 km. In a single orbit, OMI measures approximately 1650 swaths and achieves daily global coverage over 14 – 15 orbits (99 minutes per orbit). OMI measures solar backscatter within the 270-500 nm wavelength range. For this paper, we focus on the NO_2 retrieval which is derived from measurements in the 400 – 450 nm range. Since June 2007, there has been a partial blockage of the detector's full field of view, which has limited the number of valid measurements; this is known in the community as the row anomaly (RA): http://projects.knmi.nl/omi/research/product/rowanomaly-background.php.

OMI measures radiance data between the instrument's detector and the Earth's surface. Comparison of these measurements with a reference spectrum (i.e., DOAS technique), allows for calculation of the total slant column density (SCD), which represents the integrated NO_2 abundance from surface, through the atmosphere, to the instrument's detector. For tropospheric air quality studies, vertical column density (VCD) NO_2 data are more appropriate. This is done by subtracting the stratospheric slant column from the total (tropospheric + stratospheric) slant column and dividing by the tropospheric air mass factor (AMF), which is defined as the ratio of the SCD to the VCD, as shown in Eq. (1):

$$VCD_{trop} = \frac{SCD_{total} - SCD_{strat}}{AMF_{trop}} \quad \text{, where } AMF_{trop} = \frac{SCD_{trop}}{VCD_{trop}} \tag{1}$$

The tropospheric AMF has been derived to be a function of the optical atmospheric/surface properties (surface albedo, cloud fraction, and cloud height) and a priori NO_2 shape profile (Palmer et al., 2001) and can be calculated as follows (Lamsal et al., 2014) in Eq. (2):

$$AMF_{trop} = \frac{\sum_{surface}^{tropopause} SW \times x_a}{\sum_{surface}^{tropopause} x_a} \tag{2}$$

Where x_a is the partial column NO_2. The optical atmospheric/surface properties are characterized by the scattering weight (SW) and are calculated by a forward radiative transfer model (TOMRAD) in the NASA product. The SWs are then adjusted real-time by NASA depending on observed viewing angle, surface albedo, cloud fraction, and

Atmos. Chem. Phys. Discuss., doi:10.5194/acp-2017-219, 2017
Manuscript under review for journal Atmos. Chem. Phys.
Discussion started: 19 April 2017

Atmospheric Chemistry and Physics Discussions

cloud height. The a priori NO_2 shape profiles must be provided by a model simulation. In an operational setting, NASA uses the Global Model Initiative (GMI) model (1.25° lon × 1° lat; ~110 km × 110 km in the mid-latitudes) to provide the a priori NO_2 shape profiles. Instead of using a global model, we derive tropospheric VCDs using a priori NO_2 shape profiles from a regional CMAQ simulation. All other parameters from the NASA Level 2 product including total SCD, stratospheric SCD, and SW remain unchanged.

For this study, we filter the Level 2 OMI NO_2 data to ensure only valid pixels are used. We remove daily pixels with solar zenith angles ≥ 80°, cloud radiance fractions ≥ 0.5, or surface albedo ≥ 0.3. Furthermore, we remove the five largest pixels at the swath edges (i.e., pixel numbers 1 – 5 and 56 – 60). Finally, we remove any pixel flagged by NASA including pixels with NaN values, 'XTrackQualityFlags' ≠ 0 or 255 (RA flag), or 'VcdQualityFlags' > 0 and least significant bit ≠ 0 (ground pixel flag). The satellite product was oversampled for June & July over a 5-year period (2008-2012) by re-gridding to the CMAQ 1.33 km model grid and then averaging the data over the 10-month (two months × five years) period. We have chosen the June & July timeframe because the CMAQ simulation and DISOCVER-AQ Maryland data are only available during these two months.

2.2 DISCOVER-AQ NO_2 observations

In the validation of our new satellite product, we use in situ NO_2 observations from the DISCOVER-AQ Maryland field campaign. DISCOVER-AQ was a four-part field experiment designed to probe the atmosphere near urban areas in excruciating detail from aircrafts, ground station networks, and satellites. The first experimental campaign took place in Maryland (Baltimore, MD - Washington D.C. area) in July 2011. This campaign was particularly unique for an aircraft field campaign in that the focus was limited to single metropolitan area, whereas in other aircraft campaigns, spatial coverage is often over a larger domain. We utilize data acquired by three sources during this campaign: the P3-B aircraft, the ground-based Pandora spectrometer network, and the long-term EPA ground monitoring network. A typical P3-B aircraft flight path, Pandora NO_2 spectrometer locations, and ground monitor locations are shown in Figure 1. DISCOVER-AQ observations were retrieved from the online data archive: http://www-air.larc.nasa.gov/cgi-bin/ArcView/discover-aq.dc-2011. A further description of DISCOVER-AQ Maryland can be found in Crawford et al. (2014).

2.2.1 P3-B aircraft data

We use P3-B aircraft NO_2 data gathered by the Cohen group (instrument reference: (Day et al, 2002)) to assess the accuracy of our model simulation. We utilize one-minute averaged P3-B data from all fourteen flights during July 2011. One-minute averaged data is already pre-generated in the data archive. Hourly output from our model simulation is spatially and temporally matched to the observations. We then bin the data into different altitude ranges for our comparison.

Atmos. Chem. Phys. Discuss., doi:10.5194/acp-2017-219, 2017
Manuscript under review for journal Atmos. Chem. Phys.
Discussion started: 19 April 2017

2.2.2 Pandora NO_2 data

Measurements of total column NO_2 from the Pandora spectrometer (instrument reference: (Herman et al., 2009)) are used to evaluate the OMI NO_2 satellite products. Valid OMI NO_2 pixels are matched spatially and temporally to Pandora total column NO_2 observations. To smooth the data and eliminate brief small-scale plumes or anomalies, we average the Pandora observations over a two hour period (± one hour of the overpass time) before matching to the OMI NO_2 data. During July 2011, there were twelve Pandora NO_2 spectrometers operating during the experiment; this corresponded to only seventy-eight instances in which valid Pandora NO_2 observations matched valid OMI NO_2 column data.

2.2.3 EPA ground monitor data

There are eighteen EPA NO_2 monitoring sites within our area of interest that were operational during the 5-year period of interest. We gathered this data from the EPA AQS Data Mart (EPA, 2016). Monitoring data were filtered so that only days with valid satellite data were included. To smooth the data, we average all valid ground observations between 12 – 4 PM local time. All EPA monitors measure NO_2 by the chemiluminescence method which has a high bias when compared to other techniques (Dunlea et al., 2007; Lamsal et al., 2008; Lamsal et al., 2015). Dunlea et al. (2007) has shown the high bias to be 22 % in a polluted urban environment and as large as 50 % during the mid-afternoon. Lamsal et al. (2008) suggests the bias may be even higher, 50 – 65 %, in the eastern U.S. during the summertime. For this reason, we refer to NO_2 from these monitors as NO_2*.

2.3 GMI model simulation

The operational NASA OMI NO_2 product uses a Global Modeling Initiative (GMI) (Strahan et al., 2007) model simulation with a horizontal resolution of 1° × 1.25° (~110 × 110 km) to calculate a priori NO_2 shape factors. The model is driven by assimilated meteorological fields from the Goddard Earth Observing System (GEOS) at the NASA Global Modeling and Assimilation Office (GMAO, ttp://gmao.gsfc.nasa.gov/). The GEOS-5 meteorological data are provided every 3–6 h (3 h for surface fields and mixing depths) at 72 pressure levels in the vertical, extending from surface to 0.01 hPa. The model includes the latest available inventories for anthropogenic emissions as discussed in Strode et al. (2015) and Krotkov et al. (2017). These emissions are updated annually with annual scale factor estimates provided by individual countries (van Donkelaar et al., 2008). The GMI model also includes NO_x emissions from soil, lightning, biomass burning, biofuel, and aircraft sources, as described in Duncan et al. (2007) with updates as discussed in Krotkov et al. (2017). The GMI simulation is conducted for 2004-2014, sampling hourly model output at the OMI overpass time. The standard operational retrieval is based on yearly-varying monthly average NO_2 profiles derived from the GMI simulation.

2.4 CMAQ model simulation

For the high resolution OMI NO_2 product, we use a CMAQ regional model simulation initially prepared for use in Loughner et al. (2014). CMAQ v5.0 is driven off-line by meteorological inputs from the WRF model v3.3 for June

Atmos. Chem. Phys. Discuss., doi:10.5194/acp-2017-219, 2017
Manuscript under review for journal Atmos. Chem. Phys.
Discussion started: 19 April 2017

Atmospheric Chemistry and Physics Discussions

and July 2011. Anthropogenic emissions are projected to 2012 from the 2005 EPA National Emissions Inventory (NEI); the 2011 NEI was unavailable when this model simulation was originally completed. Biogenic and lightning emissions are calculated online. The 1.33 km simulation, which we use exclusively in this study, is nested inside three larger domains: 36 km, 12 km, and 4 km. Boundary conditions for the 36 km domain are provided by the MOZART-4 global model. The CMAQ 1.33 km model domain is shown in Figure 1. For additional details, including a discussion on the uncertainty of the meteorological and chemical fields in this simulation, please reference Loughner et al. (2014).

This study is particularly unique in that we use a 1.33 km simulation in lieu of a model with a horizontal resolution more typical of OMI (>13 km). We do this so that we can capture the fine-scale variability within urban areas that cannot be simulated by coarser models and observations. To ensure a fair comparison, we average model information to the pixel size. Model outputs were sampled at the local time of OMI overpass. Since monthly mean values capture the seasonal variation, we derived monthly mean values for NO_2 and temperature profiles and tropopause pressures needed for the calculation of the AMF. The exception is for June & July 2011 in which daily NO_2 profiles (e.g., (Laughner et al., 2016)) were used to calculate the AMF.

3 Results

In this section, we describe the process to develop a new high resolution satellite product and our validation efforts. First, we compare a priori NO_2 shape profiles simulated by GMI (global model) and CMAQ (regional model). Next we develop an initial OMI NO_2 satellite product (OMI_CMAQ) using AMFs generated from the CMAQ a priori NO_2 profiles. We introduce two additional steps: improving a priori NO_2 shape profiles using aircraft observations and applying a spatial weighting kernel to further improve the spatial distribution of NO_2. We then evaluate our new product by comparing to DISCOVER-AQ observations. And finally we compare the new OMI NO_2 product with NO_2 VCDs from the original CMAQ simulation.

3.1 Evaluating modeled NO_2 shape profiles: GMI vs. CMAQ

Trace gas shape profiles provided by model simulations are a critical input to satellite retrievals. To understand the effects of model choice on the a priori NO_2 shape profile, we compare the mean 2 PM local time tropospheric NO_2 vertical profiles from CMAQ and GMI at several locations in the mid-Atlantic during June & July 2011. In the left panels of Figure 2, we show the mean NO_2 mixing ratio as function of altitude for three locations: downtown Baltimore Maryland (an urban area), the Morgantown Power Plant located in Newburg, Maryland 60 km south of the District of Columbia (D.C.), and Arendtsville, Pennsylvania (rural), a location 100 km northwest of Baltimore and upwind of major metropolitan areas during days with climatologically westerly winds. All three locations are shown on Figure 1. In Baltimore, GMI simulates a mean 2 PM surface NO_2 mixing ratio of 2.2 ppbv, while CMAQ simulates 9.6 ppbv at the same location. The "Oldtown" monitoring site in Baltimore registered a NO_2* mixing ratio of 10.5 ppbv within +/- 2 hours of valid co-located satellite overpasses. As discussed in Sect. 2.2.3, the corrected surface NO_2 mixing ratio may be up to 65 % lower than observed NO_2*; our best estimate of 8.2 ppbv

Atmos. Chem. Phys. Discuss., doi:10.5194/acp-2017-219, 2017
Manuscript under review for journal Atmos. Chem. Phys.
Discussion started: 19 April 2017

with error bars [3.7, 10.6] is shown by the black triangle on Figure 2. The value simulated by CMAQ (9.6 ppbv) is much closer to the observed value than GMI (2.2 ppbv). In the second row of panels, the panels representing the Morgantown power plant, CMAQ simulates a plume of NO_2 above the surface; the max value is 11.8 ppb corresponding to an altitude of 460 m. The GMI simulation cannot resolve power plant plumes. This yields significant errors in the NO_2 shape profiles simulated by GMI near observed large point sources. In the bottom row of panels, we show a location in rural Pennsylvania. CMAQ, once again, does better in simulating the surface concentration than GMI.

However, in the free troposphere (i.e., above 3 km and below the tropopause) CMAQ consistently simulates smaller NO_2 than GMI. CMAQ simulates NO_2 mixing ratios between 0.01- 0.04 ppbv, while GMI simulates NO_2 mixing ratios between 0.06 – 0.09 ppbv over the same altitudes; GMI simulates values which are a factor of three higher than CMAQ. Both simulations include lightning NO_x. The differences likely arise from the treatment of long-range transport, which has a dominating effect at these altitudes.

3.2 Calculation of air mass factors: GMI vs. CMAQ

A normalization of the NO_2 as a function of altitude (i.e., $x_a / \Sigma x_a$ in Eq. (2)) is the next step in the calculation of the AMF; these values are defined in the literature as shape factors. The center column panels show NO_2 shape factors for three locations. In Figure 2b (Baltimore), the GMI and CMAQ shape profiles (i.e., shape factors as a function of altitude) appear to be similar, but there are noticeable differences within the boundary layer and free troposphere. In Figure 2e, there are large differences in the shape profile within the boundary layer due to CMAQ capturing a localized power plant plume. And in Figure 2h, CMAQ suggests that the NO_2 gradient near the surface is not as sharp.

Since the AMF is also a function of the SW, small differences in NO_2 shape profiles can manifest very different AMFs. For example, small differences in the shape profile at 7.5 km, where the SW is a maximum (SW = 2.9), have an order of magnitude larger effect than differences at the surface (SW = 0.4).

To fully understand the differences caused by the new NO_2 shape factors, we multiply the two shape factors by the satellite scattering weights. Here we define the shape factors × scattering weight ((i.e., $(x_a \times SW)/ \Sigma x_a$ in Eq. (2)) as the adjusted shape factors. This is analogous to the values used for calculation of the air mass factor. The AMF is the integral of the adjusted shape factors with respect to height. In Figure 2c, the CMAQ adjusted shape profile shows values much closer to zero above 3 km than GMI. By using a priori shape profiles from CMAQ, we are enhancing the sensitivity of satellite observations to NO_2 concentrations within the boundary layer in Baltimore. In Figure 2f, the adjusted shape profiles are even more dramatic. At this location, adjusted shape profile values from CMAQ are relatively large below 1 km, and close to zero above 1 km, while GMI shows nearly an order of magnitude larger sensitivity above 1 km. In Figure 2i, CMAQ shows larger values above the surface, but within the boundary layer, while GMI shows larger values directly at the surface. In areas, such as these, the adjusted shape factors yield only small changes. In Figures 2c and 2f, the area underneath the red curve is smaller than the area

underneath the blue curve. This will yield smaller AMFs when using CMAQ at these locations. As a result, we should expect the new OMI tropospheric NO_2 columns to be larger near urban areas and point sources which cannot be resolved by global models. At the rural location, the areas underneath the two curves are roughly the same, yielding similar AMFs and NO_2 columns.

3.3 Calculation of OMI tropospheric column NO_2

3.3.1 Using CMAQ profiles

We use the AMFs based off the CMAQ simulation to generate NO_2 tropospheric column amounts; we call this the OMI_CMAQ product. For this product, tropospheric NO_2 columns are calculated from the NASA Level 2 OMI NO_2 total slant column using Eq. (1). For AMFs calculated in the months of June and July 2011, we use AMFs derived from daily NO_2 shape factors as described by Laughner et al. (2016), resulting in more day-to-day variability in the AMF. Daily CMAQ NO_2 shape profiles from the hourly output are matched temporally and spatially to the OMI pixel. For years other than 2011, we use a two-month (June and July) average of the 2011 NO_2 shape factors to derive "summertime" AMFs. Since the resolution of CMAQ is finer than the resolution of OMI, we average all CMAQ AMFs across each individual pixel. Often there are over two-hundred CMAQ AMFs within a single pixel. Since CMAQ is capturing the spatial heterogeneities in urban areas, using it in lieu of GMI to provide NO_2 shape profiles can yield large variability in the AMF between adjacent OMI pixels.

Figures 3a and 3b depict the OMI NO_2 tropospheric columns using a priori shape profile information from GMI (OMI_GMI; Figure3a) and CMAQ (OMI_CMAQ; Figure 3b) in calculating the AMF. Both products are oversampled to 1.33 km for June & July over a 5-year period (2008-2012) by re-gridding to the CMAQ model grid and then averaging the data over the 10-month (two months × five years) period. We have chosen the June & July timeframe because the CMAQ simulation is only available during these two months. For the OMI_GMI product, the tropospheric NO_2 columns were taken directly from the NASA OMI NO_2 v3.0 Level 2 product. Figure 4a shows the ratio between the two products.

In the new product (OMI_CMAQ), there are large increases of the NO_2 VCDs in city centers. In the operational OMI_GMI product, over the 5-year period, the maximum tropospheric NO_2 column within Baltimore city limits is 3.9×10^{15} molecules per cm^2. By contrast, in the OMI_CMAQ product, the maximum tropospheric NO_2 column within Baltimore city limits is 7.2×10^{15} molecules per cm^2. These results indicate that by using a regional model, the tropospheric NO_2 VCDs in urban areas rise dramatically. This is due, in part, to the regional model being able to better capture NO_2 concentrations in the lower-most part of the troposphere (i.e., Figure 2). In suburban and rural locations, NO_2 tropospheric VCDs are roughly the same. For example, at the rural Pennsylvania (Arendtsville) location, the NO_2 tropospheric vertical column in the operational product is 2.8×10^{15} molecules per cm^2 and 2.7×10^{15} molecules per cm^2 in the new OMI_CMAQ product.

Atmos. Chem. Phys. Discuss., doi:10.5194/acp-2017-219, 2017
Manuscript under review for journal Atmos. Chem. Phys.
Discussion started: 19 April 2017

Atmospheric Chemistry and Physics Discussions

3.3.2 Improving modeled vertical profile information with in situ observations

While using CMAQ to calculate AMFs yields a marked improvement in simulating profile shape when compared to using GMI, this CMAQ simulation has a high bias in the calculation of total reactive nitrogen oxides (NO_y) (Goldberg et al., 2014; Anderson et al., 2014), which must be accounted for. Many literature sources, including others using different model set-ups (all are based on the NEI), also show a high bias in simulating summertime column NO_2 (Canty et al., 2015; Souri et al., 2016), NO_x (Travis et al., 2016), and NO_y (Goldberg et al., 2016).

In Figure 5, we show NO_2 observations acquired by the P3-B aircraft in the early afternoon between 300 m and 3 km during DISCOVER-AQ Maryland and matched CMAQ output. NO_2 mixing ratios simulated by CMAQ are consistently smaller throughout the mid- and upper-boundary layer and lower free troposphere (1 – 3 km) by up to a factor of three, but there is fairly good agreement below 1 km; similar results were found by Flynn et al. (2016).

Since the P3-B aircraft has limited measurements above 3 km, we have to use estimates from other literature sources to determine the validity of CMAQ in the free troposphere. Lamsal et al. (2017) used measurements from the Airborne Compact Atmospheric Mapper (ACAM) to deduce that GMI is better than CMAQ at simulating NO_2 in the free troposphere. In the upper free troposphere, above 10.5 km, Travis et al. (2016) note that NO_2 is significantly underestimated by global models, such as GMI. As shown in Figure 2, CMAQ simulates even lower NO_2 concentrations than GMI at these altitudes.

We apply a scaling factor inferred from in situ aircraft observations to account for the high model bias below 3 km, and low model bias above 3 km; this is a rudimentary form of data assimilation. Below 3 km, the model was scaled to observations from the P3-B by multiplying the original values at these altitudes by the fraction of NO_2 actually observed. For example, modeled NO_2 between 1000 – 1500 m was multiplied by 0.63 to account for the model high bias within this altitude bin. This procedure was repeated for all altitude bins in 500-m intervals from the surface up to 3 km. It should be noted that aircraft measurements from the DISCOVER-AQ Maryland campaign took place only within the Baltimore metropolitan region, and thus these scaling factors may not be fully applicable to upwind rural regions, and certainly cannot be applied to locations outside the eastern United States. Between the altitudes of 3 km – 10.5 km, we switched out the NO_2 mixing ratios from CMAQ for NO_2 mixing ratios from GMI. Between 10.5 km and the tropopause, we use GMI NO_2 mixing ratios multiplied by a factor of three; this scaling factor is based on summertime NO_2 observations during the SEAC^{4}RS field campaign as described by Travis et al. (2016).

Using these scaled mixing ratios, we then re-calculate the AMFs and corresponding tropospheric NO_2 columns. Figure 3c shows observationally-constrained OMI_CMAQ (OMI_CMAQ_O) tropospheric NO_2 columns during the same 5-year summertime period. NO_2 tropospheric columns in this product are smaller in magnitude than OMI_CMAQ, and yet still noticeably larger in urban areas than the operational OMI_GMI retrieval (i.e., in Baltimore OMI_GMI: 3.9×10^{15} , OMI_CMAQ: 7.2×10^{15}, OMI_CMAQ_O: 5.0×10^{15}). Retrievals in upwind rural areas in this new product are now lower than the operational product (i.e., in Arendtsville OMI_GMI: 2.8×10^{15} , OMI_CMAQ: 2.7×10^{15}, OMI_CMAQ_O: 1.7×10^{15}).

Atmos. Chem. Phys. Discuss., doi:10.5194/acp-2017-219, 2017
Manuscript under review for journal Atmos. Chem. Phys.
Discussion started: 19 April 2017

Atmospheric Chemistry and Physics Discussions

3.3.3 Enhancing spatial resolution with spatial weighting kernels

Finally in a last step, we apply the method described by Kim et al. (2016) to downscale the OMI retrieval. This method applies a spatial-weighting kernel to portions of each pixel based on the estimated influence from each locality within the pixel. For example, if one side of a pixel overlaps a polluted region, while the other side of the pixel overlaps a cleaner area, the operational OMI product will denote that the entire area is moderately polluted. Instead, we weight portions of the individual pixel based on the variability simulated in CMAQ. Using this method, the quantity of the satellite data is numerically preserved. This yields a higher resolution snapshot of tropospheric column NO_2 that is still constrained by satellite data. Please reference Kim et al. (2016) for a visual representation of this method.

We call this product OMI_CMAQ observationally-constrained + downscaled (OMI_CMAQ_OD). Figure 3d shows OMI_CMAQ_OD tropospheric NO_2 columns. There is now large variability throughout the region, which is typical of a pollutant with a short lifetime (< 1 day) such as NO_2 in the summertime. NO_2 tropospheric columns in urban cores are now significantly larger than the operational product, (i.e., in Baltimore OMI_GMI: 3.9×10^{15}, OMI_CMAQ_OD: 10.2×10^{15}). The largest increases occur near power plants, cement kilns, and major highways. OMI_CMAQ_OD in upwind rural areas are 20 – 50 % lower than the operational product (i.e., in Arendtsville OMI_GMI: 2.8×10^{15}, OMI_CMAQ_OD: 1.6×10^{15}).

We must clarify, however, that these results are only applicable for our region of interest. While we find that rural areas within our mid-Atlantic model domain now have tropospheric NO_2 columns which are 20 – 50 % lower than the operational product, we cannot conclude that this would be the same elsewhere. The "rural" locations within our model domain are situated in a particularly precarious spot because they are close, but not too close to major urban areas. These sites are only "rural" in the sense that there are no major metropolitan areas within 200 km upwind of them. Because Arendtsville lies within 50 km of Harrisburg and 100 km of Baltimore, a GMI simulation with a resolution of 1.25° × 1° (~110 × 110 km) will group this location into a grid cell also including Harrisburg and portions of Baltimore; both of which are not rural. Therefore a location that is 100's of kilometers from the nearest city and with spatial homogeneity may be simulated with fidelity by GMI and therefore the operational OMI product may be an accurate representation of reality in these cases.

While this new product shows power plant plumes that are two to three times larger, we are not suggesting that emissions from power plants are larger than we thought. Instead we are suggesting that OMI can now "see" these individual plumes, where as in the operational product, these plumes are blended into an average across the entire OMI pixel. In rare cases, oversampling the operational product in and around very large rural point sources, can denote large power plant plumes (deFoy et al., 2015), but up until this point, smaller point sources or localized sources near major urban areas could not be seen by OMI.

Atmos. Chem. Phys. Discuss., doi:10.5194/acp-2017-219, 2017
Manuscript under review for journal Atmos. Chem. Phys.
Discussion started: 19 April 2017

Atmospheric Chemistry and Physics Discussions

3.4 Comparison of satellite products to in situ observations

To determine the accuracy of the new products, we compare the products to independent NO_2 observations. During DISCOVER-AQ Maryland, total column NO_2 was measured by a network of twelve Pandora instruments (Herman et al., 2009). We match daily valid Pandora NO_2 and valid satellite overpass information, and plot the information in Figure 6a. To calculate total OMI columns, we add the vertical stratospheric column information, a variable in the NASA OMI NO_2 Level 2 files, to the OMI tropospheric retrievals. While the operational product (OMI_GMI) shows some agreement at low values, it has poor agreement when observed NO_2 column amounts are greater than 10×10^{15} cm^{-2}. This is due to coarse resolution of OMI pixels (24 × 13 km at nadir) and the AMFs computed with GMI a priori NO_2 profiles, among potential other factors. The slope of the OMI_GMI best-fit line is 0.45, representing a striking low bias at high values, and the $r^2 = 0.09$ denoting almost no correlation; similar results were found by Ialongo et al. (2016).

Table 1 shows the statistical comparison between the satellite products and observations. All OMI_CMAQ products yield slopes closer to one indicating that they are better at capturing the variability between low and high values observed by the ground monitors. The OMI_CMAQ_OD product eliminates the bias altogether. The slope of the OMI_CMAQ_OD best-fit is 1.02 and the r^2 increases. An improved but still low r^2-value in the newest product may indicate that a 1.33 km CMAQ simulation provides an improvement, but not an identical match, of daily NO_x emissions and fine-scale winds responsible for plume dispersion. Furthermore, we cannot expect the satellite to match the exact spatial heterogeneity observed by the point measurements from Pandora.

The long-term EPA monitoring network provides surface observations outside the July 2011 timeframe. In Figure 6b, we compare mean NO_2* at each monitoring site to the two satellite products. All valid NO_2* data at each monitoring site over a 5-year (2008-2012) 2-month (June & July) period are averaged into a single point (up to 305 data entries) and is matched to an average of satellite data over the same time period. The correlation between OMI_GMI and surface observations is $r^2 = 0.39$, while the correlation between OMI_CMAQ_OD and surface observations is $r^2 = 0.60$, a substantial improvement. This suggests that a high resolution satellite product with improved AMFs, will be able to detect surface NO_2 concentrations with more accuracy. As shown in Table 1, OMI_CMAQ without observational constraints performs almost as good ($r^2 = 0.55$); this is especially encouraging since comprehensive field measurements, such as those from DISCOVER-AQ, are limited in spatial and temporal scope.

3.5 OMI_CMAQ vs. CMAQ

We can now more fairly assess the NO_2 columns simulated by CMAQ using a high resolution OMI NO_2 product. In Figure 7, we show a comparison between CMAQ and OMI_CMAQ_OD. Only model data within +/- 1 hour of and co-located with valid overpass data is shown in order to remove biases during cloudy days or days with invalid data. We see a consistent model low bias in rural areas, and consistent model high bias in urban areas. Interestingly the high bias is larger in the immediate Baltimore metropolitan area compared to the D.C. metropolitan region.

Atmos. Chem. Phys. Discuss., doi:10.5194/acp-2017-219, 2017
Manuscript under review for journal Atmos. Chem. Phys.
Discussion started: 19 April 2017

Atmospheric Chemistry and Physics Discussions

We attribute the model low bias in rural regions to several shortcomings of this model simulation. This simulation did not include NO_x emissions from soils. Rasool et al. (2016) has shown soil NO_x emissions to be particularly important in the central United States, with a lesser role in the eastern United States. Excluding these emissions may have resulted in less NO_x being transported from upwind regions. This model simulation utilized CB05 gas-phase chemistry, which is known to underestimate the recycling of alkyl nitrates back to NO_2 (Hildebrandt-Ruiz and Yarwood, 2013; Canty et al., 2015). CB05e51 gas-phase chemistry, released in a newer version of CMAQ (https://www.airqualitymodeling.org/in-dex.php/CMAQ_v5.1_CB05_updates), better handles alkyl nitrates and employs faster recycling of short-lived alkyl nitrate species. Faster recycling of alkyl nitrates would yield higher NO_2 concentrations throughout the modeling domain. Travis et al. (2016) found that upper tropospheric NO_x is too low when compared to observations from aircraft during SEAC^{4}RS. This is possibly due to downward stratospheric transport, outflow from convection, or OH chemistry that is not characterized correctly by models. Lightning NO_x is still a very active area of research (Pickering et al., 2016). Although this model simulation did include lightning NO_x emissions, there is a possibility these emissions are underestimated.

We attribute the model high bias in urban regions to an overestimate of anthropogenic NO_x emissions (Anderson et al., 2014; Souri et al., 2016). This may be due to an improper allocation of area and mobile (on-road and off-road) source emissions which are spatially distributed based on population and number of cars respectively, or quite simply an overestimate of these sector emissions. Quantifying the uncertainty in MOVES, the mobile emissions software, is an active area of research.

3.6 Comparison of model to satellite and in situ observations

To further evaluate the model, we compare the model simulation to DISCOVER-AQ and EPA observations. In Figure 8a, we show a Pandora NO_2 comparison in the same manner as Figure 6a. In addition to showing CMAQ, we also show OMI_CMAQ_OD. We add the stratospheric VCD information from the OMI NO_2 Level 2 product to the CMAQ tropospheric columns to ensure a fair comparison. Both the model and new OMI NO_2 product have a slope close to unity indicating that both are able to match the variability in NO_2 columns. There is, however, a consistent low offset. This may indicate that the stratospheric VCD in the NASA Level 2 retrieval may be too low during this two-month timeframe. The r^2 of CMAQ is higher than OMI_CMAQ_OD. This is not particularly surprising because the resolution of the satellite is coarse, despite it being processed with new air mass factors.

In Figure 8b, we show a comparison between CMAQ, OMI_CMAQ_OD and ground monitors. The r^2 between CMAQ and ground monitors to be 0.70, while the correlation with the new satellite product is 0.73. The OMI_CMAQ_OD product has a better correlation with ground NO_2 monitors than the 1.33 km CMAQ simulation alone indicating that there is added utility in the satellite data.

Atmos. Chem. Phys. Discuss., doi:10.5194/acp-2017-219, 2017
Manuscript under review for journal Atmos. Chem. Phys.
Discussion started: 19 April 2017

4 Summary and conclusions

This study demonstrates the critical importance of using high resolution a priori NO_2 shape factors to develop AMFs in and around metropolitan areas. We develop three new OMI NO_2 products: using high spatial resolution NO_2 profiles from a 1.33 km CMAQ model simulation (OMI_CMAQ), using CMAQ profiles constrained by in-situ observations (OMI_CMAQ_O), and applying model-derived spatial information (downscaling) to OMI_CMAQ_O (OMI_CMAQ_OD). When using high spatial resolution models to develop the AMF, the mean AMF in urban areas decreases by up to 50 % causing the tropospheric VCDs in urban areas to increase by up to a factor of two. This is because high resolution models simulate larger concentrations near the surface in urban areas. In essence, we are reprocessing the satellite to look for NO_2 closer to the surface than in the original product. We believe this finding extends to other urban areas since coarse global models will consistently merge rural and urban pollution, and subsequently overestimate the AMF in city centers.

Another novel step in our re-processing technique is using in situ observations to enhance modeled NO_2 profile shapes. CMAQ NO_2 values in the Baltimore-Washington metropolitan region are generally too large within the boundary layer, too small in the mid-troposphere, and a factor of three too small in the uppermost troposphere. This may not be fully applicable to rural regions, since the DISCOVER-AQ field campaign was only focused in the urban corridor. As a result, our adjusted satellite product in rural regions must be taken with some uncertainty. With that said, constraining model simulations to observations yields an improved satellite product over the non-constrained product when comparing to Pandora NO_2. Furthermore, by constraining to observations, we reduce the dependence on a priori emission inventories (e.g., NEI) used in model simulations, which can have deficiencies (Anderson et al., 2014; Souri et al., 2016; Travis et al., 2016). For example, in the constraint-based product, VCDs in Baltimore are 30 % lower than the OMI_CMAQ product. The tropospheric VCDs in rural Mid-Atlantic areas are 20 – 50 % lower than both the OMI_CMAQ and operational products.

Lastly, we apply a technique developed by Kim et al. (2016) to downscale OMI NO_2 data. This technique is especially valuable for pollutant exposure health studies, which require high resolution long-term pollutant estimates. The downscaling procedure provides a higher spatial resolution snapshot of NO_2, while not altering the observed satellite pixel values. Instead this technique re-allocates values across the pixel based on the variability within the high resolution model. As a result, the new satellite product (OMI_CMAQ_OD) shows higher values in urban, polluted areas and lower values in rural, unpolluted areas than the operational OMI_GMI product. This new product better captures the urban-scale variability of NO_2 and has a much better correlation with ground monitors. A deficiency with this technique is that if a localized source, such as a power plant plume or wildfire, is not simulated at all by the model, then this error will be passed on to the product. Therefore, we do not recommend using the downscaling technique in areas where the emission inventory is very uncertain.

The refined OMI_CMAQ_OD product provides a better NO_2 column measurement when compared to Pandora column NO_2: the slope is near unity and the r^2 increases over the operational OMI NO_2 product. An important finding of this work is that using a high resolution model, not the constraining to observations, provides the majority

of the improvement, when comparing to ground monitors. This suggests that a high resolution model with reasonable fidelity can be used anywhere in the world, and is not tied into an area in which a field experiment is located.

This technique can be used as a bridge until newer instruments such as TROPOMI are instituted. Future instruments will have increased spatial resolution, but comparison to OMI without using this technique may yield large differences around urban areas. At the same time, we demonstrate the importance of using a high resolution model simulation for retrievals from future satellite missions. A combination of both increased satellite resolution and model resolution are needed in order to improve NO_2 satellite retrievals. We urge other community members to generate high resolution OMI NO_2 data using this technique if it is to be used for small-scale (< 100 km length scale) studies as it provides a better alternative for urban areas than standard satellite products.

Acknowledgments

This work was supported by the EPA SEARCH (Solutions for Energy, AiR, Climate, and Health) Air, Climate, and Energy (ACE) Center based at Yale University and led by Michelle Bell and co-led by Benjamin Hobbs of Johns Hopkins University. We would like to thank Ron Cohen and his research group for their observations NO_2 from the P3-B aircraft during DISCOVER-AQ Maryland. We would also like to thank Jay Herman and his research group for their Pandora NO_2 measurements during this same time period. All data from DISCOVER-AQ Maryland can be downloaded freely from http://www-air.larc.nasa.gov/cgi-bin/ArcView/discover-aq.dc-2011. EPA NO_2* data was downloaded from the AQS Data Mart, and can be freely retrieved from: https://aqs.epa.gov/aqsweb/documents/data_mart_wel-come.html. We would also like to thank Chinmay Satam for preparation of the emissions in the CMAQ model simulation. We acknowledge the free use of NO_2 column data from the OMI sensor available at: https://disc.gsfc.nasa.gov/Aura/data-holdings/OMI/omno2_v003.shtml. Argonne National Laboratory is operated by UChicago Argonne, LLC, under contract no. DE-AC2-06CH11357 with the U.S. Department of Energy. This publication was developed under Assistance Agreement No. RD835871 awarded by the U.S. Environmental Protection Agency to Yale University. It has not been formally reviewed by EPA. The views expressed in this document are solely those of the authors and do not necessarily reflect those of the Agency. EPA does not endorse any products or commercial services mentioned in this publication.

Atmos. Chem. Phys. Discuss., doi:10.5194/acp-2017-219, 2017
Manuscript under review for journal Atmos. Chem. Phys.
Discussion started: 19 April 2017

Atmospheric Chemistry and Physics Discussions

References

Allen, D. J., Pickering, K. E., Pinder, R. W., Henderson, B. H., Appel, K. W., and Prados, A.: Impact of lightning-NO on eastern United States photochemistry during the summer of 2006 as determined using the CMAQ model, Atmos. Chem. Phys., 12, 1737-1758, 2012.

Anderson, D. C., Loughner, C. P., Diskin, G., Weinheimer, A., Canty, T. P., Salawitch, R. J., Worden, H. M., Fried, A., Mikoviny, T., Wisthaler, A., and Dickerson, R. R.: Measured and modeled CO and NOy in DISCOVER-AQ: An evaluation of emissions and chemistry over the eastern US, Atmos. Environ., 96, 78-87, 2014.

Bechle, M. J., Millet, D. B., and Marshall, J. D.: National Spatiotemporal Exposure Surface for NO_2: Monthly Scaling of a Satellite-Derived Land-Use Regression, 2000–2010, Environ. Sci. & Tech., 49, 12297-12305, 2015.

Beirle, S., Boersma, K. F., Platt, U., Lawrence, M. G., and Wagner, T.: Megacity Emissions and Lifetimes of Nitrogen Oxides Probed from Space, Science, 333, 1737-1739, 2011.

Boersma, K. F., Eskes, H. J., Veefkind, J. P., Brinksma, E. J., Van Der A, R. J., Sneep, M., Van Der Oord, G. H. J., Levelt, P. F., Stammes, P., and Gleason, J. F.: Near-real time retrieval of tropospheric NO_2 from OMI, Atmos. Chem. Phys., 7, 2103-2118, 2007.

Boersma, K. F., Jacob, D. J., Eskes, H. J., Pinder, R. W., and Wang, J.: Intercomparison of SCIAMACHY and OMI tropospheric NO_2 columns: Observing the diurnal evolution of chemistry and emissions from space, J. Geophys. Res. Atmos., 113, 2008a.

Boersma, K. F., Jacob, D. J., Bucsela, E. J., Perring, A. E., Dirksen, R., Yantosca, R. M., Park, R. J., Wenig, M. O., Bertram, T. H., and Cohen, R. C.: Validation of OMI tropospheric NO_2 observations during INTEX-B and application to constrain NOx emissions over the eastern United States and Mexico, Atmos. Environ., 42, 4480-4497, 2008b.

Boersma, K. F., Vinken, G. C. M., and Tournadre, J.: Ships going slow in reducing their NOx emissions: changes in 2005–2012 ship exhaust inferred from satellite measurements over Europe, Environ. Res. Lett., 10, 074007, 2015.

Bovensmann, H., Burrows, J. P., Buchwitz, M., Frerick, J., Noël, S., Rozanov, V. V., Chance, K. V., and Goede, A. P. H.: SCIAMACHY: Mission objectives and measurement modes, J. Atmos. Sci., 56, 127-150, 1999.

Bucsela, E. J., Celarier, E. A., Wenig, M. O., Gleason, J. F., Veefkind, J. P., Boersma, K. F., and Brinksma, E. J.: Algorithm for NO_2 Vertical Column Retrieval From the Ozone Monitoring Instrument, IEEE Transactions on Geoscience and Remote Sensing, 44, 1245-1258, 2006.

Burrows, J. P., Weber, M., Buchwitz, M., Rozanov, V., Ladstätter-Weißenmayer, A., Richter, A., DeBeek, R., Hoogen, R., Bramstedt, K., and Eichmann, K.-U.: The global ozone monitoring experiment (GOME): Mission concept and first scientific results, J. Atmos. Sci., 56, 151-175, 1999.

Canty, T. P., Hembeck, L., Vinciguerra, T. P., Anderson, D. C., Goldberg, D. L., Carpenter, S. F., Allen, D. J., Loughner, C. P., Salawitch, R. J., and Dickerson, R. R.: Ozone and NOx chemistry in the eastern US: evaluation of CMAQ/CB05 with satellite (OMI) data, Atmos. Chem. Phys., 15, 10965-10982, 2015.

Chen, D., Zhou, B., Beirle, S., Chen, L. M., and Wagner, T.: Tropospheric NO2 column densities deduced from zenith-sky DOAS measurements in Shanghai, China, and their application to satellite validation, Atmos. Chem. Phys., 9, 3641-3662, 2009.

Conrad, R.: Soil microorganisms as controllers of atmospheric trace gases (H_2, CO, CH_4, OCS, N_2O, and NO)., Microbiological reviews, 60, 609-640, 1996.

Crawford, J. H., Dickerson R. R., and Hains, J.: DISCOVER-AQ: Observations and early results, Environmental Manager, 8-15, 2014.

Curier, R. L., Kranenburg, R., Segers, A. J. S., Timmermans, R. M. A., and Schaap, M.: Synergistic use of OMI NO_2 tropospheric columns and LOTOS–EUROS to evaluate the NOx emission trends across Europe, Remote Sensing of Environment, 149, 58-69, 2014.

Day, D. A., Wooldridge, P. J., Dillon, M. B., Thornton, J. A., and Cohen, R. C.: A thermal dissociation laser-induced fluorescence instrument for in situ detection of NO_2, peroxy nitrates, alkyl nitrates, and HNO_3, J. Geophys. Res. Atmos., 107, ARTN 4046, 2002.

de Foy, B., Lu, Z., Streets, D. G., Lamsal, L. N., and Duncan, B. N.: Estimates of power plant NOx emissions and lifetimes from OMI NO_2 satellite retrievals, Atmos. Environ., 116, 1-11, 2015.

Duncan, B. N., Strahan, S. E., Yoshida, Y., Steenrod, S. D., and Livesey, N.: Model study of the cross-tropopause transport of biomass burning pollution, Atmos. Chem. Phys., 7, 3713-3736, 2007.

Duncan, B. N., Lamsal, L. N., Thompson, A. M., Yoshida, Y., Lu, Z., Streets, D. G., Hurwitz, M. M., and Pickering,

K. E.: A space based, high resolution view of notable changes in urban NOx pollution around the world (2005–2014), J. Geophys. Res. Atmos., 121, 976-996, 2016.

Dunlea, E. J., Herndon, S. C., Nelson, D. D., Volkamer, R. M., San Martini, F., Sheehy, P. M., Zahniser, M. S., Shorter, J. H., Wormhoudt, J. C., and Lamb, B. K.: Evaluation of nitrogen dioxide chemiluminescence monitors in a polluted urban environment, Atmos. Chem. Phys., 7, 2691-2704, 2007.

EPA: AQS Data Mart, 2016. https://aqs.epa.gov/aqsweb/documents/data_mart_welcome.html

Flynn, C. M., Pickering, K. E., Crawford, J. H., Lamsal, L., Krotkov, N., Herman, J., Weinheimer, A., Chen, G., Liu, X., and Szykman, J.: Relationship between column-density and surface mixing ratio: Statistical analysis of O_3 and NO_2 data from the July 2011 Maryland DISCOVER-AQ mission, Atmos. Environ., 92, 429-441, 2014.

Flynn, C. M., Pickering, K. E., Crawford, J. H., Weinheimer, A., Diskin, G., Thornhill, K. L., Loughner, C., Lee, P., and Strode, S.: Variability of O_3 and NO_2 profile shapes during DISCOVER-AQ: Implications for satellite observations and comparisons to model-simulated profiles, Atmos. Environ., 147, 133-156, 2016.

Goldberg, D. L., Loughner, C. P., Tzortziou, M., Stehr, J. W., Pickering, K. E., Marufu, L. T., and Dickerson, R. R.: Higher surface ozone concentrations over the Chesapeake Bay than over the adjacent land: Observations and models from the DISCOVER-AQ and CBODAQ campaigns, Atmos. Environ., 84, 9-19, 2014.

Goldberg, D. L., Vinciguerra, T. P., Anderson, D. C., Hembeck, L., Canty, T. P., Ehrman, S. H., Martins, D. K., Stauffer, R. M., Thompson, A. M., Salawitch, R. J., and Dickerson, R. R.: CAMx Ozone Source Attribution in the Eastern United States using Guidance from Observations during DISCOVER AQ Maryland, Geophys. Res. Lett., 43, 2016.

Han, K. M., Lee, S., Chang, L. S., and Song, C. H.: A comparison study between CMAQ-simulated and OMI-retrieved NO_2 columns over East Asia for evaluation of NOx emission fluxes of INTEX-B, CAPSS, and REAS inventories, Atmos. Chem. Phys., 15, 1913-1938, 2015.

Herman, J., Cede, A., Spinei, E., Mount, G., Tzortziou, M., and Abuhassan, N.: NO_2 column amounts from ground-based Pandora and MFDOAS spectrometers using the direct-sun DOAS technique: Intercomparisons and application to OMI validation, J. Geophys. Res., 114, D13307, 2009.

Heue, K.-P., Wagner, T., Broccardo, S. P., Walter, D., Piketh, S. J., Ross, K. E., Beirle, S., and Platt, U.: Direct observation of two dimensional trace gas distributions with an airborne Imaging DOAS instrument, Atmos. Chem. Phys., 8, 6707-6717, 2008.

Hilboll, A., Richter, A., and Burrows, J. P.: Long-term changes of tropospheric NO_2 over megacities derived from multiple satellite instruments, Atmos. Chem. Phys., 13, 4145-4169, 2013.

Hildebrandt-Ruiz, L., and Yarwood, G.: Interactions between organic aersol and NOy: influence on oxidant production, 2013.

Hudman, R. C., Russell, A. R., Valin, L. C., and Cohen, R. C.: Interannual variability in soil nitric oxide emissions over the United States as viewed from space, Atmos. Chem. Phys., 10, 9943-9952, 2010.

Huijnen, V., Eskes, H. J., Poupkou, A., Elbern, H., Boersma, K. F., Foret, G., Sofiev, M., Valdebenito, A., Flemming, J., Stein, O., Gross, A., Robertson, L., D'Isidoro, M., Kioutsioukis, I., Friese, E., Amstrup, B., Bergstrom, R., Strunk, A., Vira, J., Zyryanov, D., Maurizi, A., Melas, D., Peuch, V.-H., and Zerefos, C.: Comparison of OMI NO_2 tropospheric columns with an ensemble of global and European regional air quality models, Atmos. Chem. Phys., 10, 3273-3296, doi:10.5194/acp-10-3273-2010, 2010.

Ialongo, I., Herman, J., Krotkov, N., Lamsal, L., Boersma, K. F., Hovila, J., and Tamminen, J.: Comparison of OMI NO_2 observations and their seasonal and weekly cycles with ground-based measurements in Helsinki, Atmos. Meas. Tech., 9, 5203, 2016.

Kim, H. C., Lee, P., Judd, L., Pan, L., and Lefer, B.: OMI NO_2 column densities over North American urban cities: the effect of satellite footprint resolution, Geosci. Mod. Dev., 9, 1111-1123, 2016.

Krotkov, N. A., McLinden, C. A., Li, C., Lamsal, L. N., Celarier, E. A., Marchenko, S. V., Swartz, W. H., Bucsela, E. J., Joiner, J., and Duncan, B. N.: Aura OMI observations of regional SO_2 and NO_2 pollution changes from 2005 to 2014, Atmos. Chem. Phys., 16, 4605-4629, 2016.

Krotkov, N. A., Lamsal, L. N., Celarier, E. A., Swartz, W. H., Marchenko, S. V., Bucsela, E. J., Chan, K. L., and Wenig, M. O.: Version 3 OMI NO_2 Standard Product, Atmos. Meas. Tech. Discuss., 2017.

Kuhlmann, G., Lam, Y. F., Cheung, H. M., Hartl, A., Fung, J. C. H., Chan, P. W., and Wenig, W. O.: Development of a custom OMI NO_2 data product for evaluating biases in a regional chemistry transport model, Atmos. Chem. Phys., 15, 5627-5644, 2015.

Lamsal, L. N., Martin, R. V., van Donkelaar, A., Steinbacher, M., Celarier, E. A., Bucsela, E., Dunlea, E. J., and Pinto, J. P.: Ground-level nitrogen dioxide concentrations inferred from the satellite-borne Ozone Monitoring Instrument, J. Geophys. Res., 113, D16308, 2008.

Lamsal, L. N., Krotkov, N. A., Celarier, E. A., Swartz, W. H., Pickering, K. E., Bucsela, E. J., Gleason, J. F.,

Martin, R. V., Philip, S., and Irie, H.: Evaluation of OMI operational standard NO_2 column retrievals using in situ and surface-based NO_2 observations, Atmos. Chem. Phys., 14, 11587-11609, 2014.

Lamsal, L. N., Duncan, B. N., Yoshida, Y., Krotkov, N. A., Pickering, K. E., Streets, D. G., and Lu, Z.: US NO_2 trends (2005 - 2013): EPA Air Quality System (AQS) data versus improved observations from the Ozone Monitoring Instrument (OMI), Atmos. Environ., 110, 130-143, 2015.

Lamsal, L. N., Janz, S. J., Krotkov, N. A., Pickering, K. E., Spurr, R. J. D., Kowalewski, M. G., Loughner, C. P., Crawford, J. H., Swartz, W. H., and Herman, J. R.: High-resolution NO_2 observations from the Airborne Compact Atmospheric Mapper: Retrieval and validation, J. Geophys. Res. Atmos., 122, 1953-1970, 2017.

Laughner, J. L., Zare, A., and Cohen, R. C.: Effects of daily meteorology on the interpretation of space-based remote sensing of NO_2, Atmos. Chem. Phys., 16, 15247-15264, 2016.

Lee, H. J., and Koutrakis, P.: Daily ambient NO_2 concentration predictions using satellite ozone monitoring instrument NO_2 data and land use regression, Environ. Sci. & Tech., 48, 2305-2311, 2014.

Levelt, P. F., Van den Oord, G. H. J., Dobber, M. R., Malkki, A., Visser, H., de Vries, J., Stammes, P., Lundell, J. O. V., and Saari, H.: The Ozone Monitoring Instrument, IEEE Trans. Geosci. Rem. Sens., 44, 1093-1101, 2006.

Liaskos, C. E., Allen, D. J., and Pickering, K. E.: Sensitivity of tropical tropospheric composition to lightning NOx production as determined by replay simulations with GEOS-5, J. Geophys. Res. Atmos., 2015.

Lin, J. T., Liu, M. Y., Xin, J. Y., Boersma, K. F., Spurr, R., Martin, R., and Zhang, Q.: Influence of aerosols and surface reflectance on satellite NO_2 retrieval: seasonal and spatial characteristics and implications for NOx emission constraints, Atmos. Chem. Phys, 15, 11217-11241, 2015.

Loughner, C. P., Tzortziou, M., Follette-Cook, M., Pickering, K. E., Goldberg, D., Satam, C., Weinheimer, A., Crawford, J. H., Knapp, D. J., and Montzka, D. D.: Impact of bay breeze circulations on surface air quality and boundary layer export, J. Appl. Meteorol. Climatol., 53, 1697-1713, 2014.

Lu, Z., and Streets, D. G.: Increase in NOx emissions from Indian thermal power plants during 1996–2010: unit-based inventories and multisatellite observations, Environ. Sci. & Tech., 46, 7463-7470, 2012.

Lu, Z., Streets, D. G., de Foy, B., Lamsal, L. N., Duncan, B. N., and Xing, J.: Emissions of nitrogen oxides from US urban areas: estimation from Ozone Monitoring Instrument retrievals for 2005–2014, Atmos. Chem. Phys., 15, 10367-10383, 2015.

Ma, J. Z., Beirle, S., Jin, J. L., Shaiganfar, R., Yan, P., and Wagner, T.: Tropospheric NO2 vertical column densities over Beijing: results of the first three years of ground-based MAX-DOAS measurements (2008–2011) and satellite validation, Atmos. Chem. Phys., 13, 1547-1567, 2013.

Martin, R. V., Chance, K., Jacob, D. J., Kurosu, T. P., Spurr, R. J. D., Bucsela, E., Gleason, J. F., Palmer, P. I., Bey, I., and Fiore, A. M.: An improved retrieval of tropospheric nitrogen dioxide from GOME, J. Geophys. Res. Atmos., 107, 2002.

Martin, R. V., Jacob, D. J., Chance, K., Kurosu, T. P., Palmer, P. I., and Evans, M. J.: Global inventory of nitrogen oxide emissions constrained by space-based observations of NO_2 columns, J. Geophys. Res. Atmos., 108, 2003.

McLinden, C. A., Fioletov, V., Krotkov, N. A., Li, C., Boersma, K. F., and Adams, C.: A Decade of Change in NO_2 and SO_2 over the Canadian Oil Sands As Seen from Space, Environ. Sci. & Tech., 50, 331-337, 2015.

Novotny, E. V., Bechle, M. J., and Millet, D. B., and Marshall, J. D.: National satellite-based land-use regression: NO_2 in the United States, Environ. Sci. & Tech., 45, 4407-4414, 2011.

Palmer, P. I., Jacob, D. J., Chance, K. V., Martin, R. V., Spurr, R. J. D., Kurosu, T., Bey, I., Yantosca, R. M., Fiore, A., and Li, Q.: Air mass factor formulation for spectroscopic measurements from satellites: Application to formaldehyde retrievals from the Global Ozone Monitoring Experiment, J. Geophys. Res., 106, 14539-14550, 2001.

Pickering, K. E., Bucsela, E., D, Ring, A., Holzworth, R., and Krotkov, N.: Estimates of lightning NOx production based on OMI NO_2 observations over the Gulf of Mexico, J. Geophys. Res. Atmos., 121, 8668-8691, 2016.

Platt, U.: Differential optical absorption spectroscopy (DOAS), Air monitoring by spectroscopic technique, 127, 27-84, 1994.

Pujadas, M., Núñez, L., and Lubrani, P.: Assessment of NO_2 satellite observations for en-route aircraft emissions detection, Remote Sensing of Environment, 115, 3298-3312, 2011.

Rasool, Q. Z., Zhang, R., Lash, B., and Cohan, D. S., Cooter, E. J., Bash, J. O., Lamsal, L. N.: Enhanced representation of soil NO emissions in the Community Multiscale Air Quality (CMAQ) model version 5.0. 2, Geosci. Mod. Dev., 9, 3177-3197, 2016.

Ridley, B. A., Dye, J. E., Walega, J. G., Zheng, J., Grahek, F. E., and Rison, W.: On the production of active nitrogen by thunderstorms over New Mexico, J. Geophys. Res. Atmos., 101, 20985-21005, 1996.

Russell, A. R., Perring, A. E., Valin, L. C., Bucsela, E. J., Browne, E. C., Wooldridge, P. J., and Cohen, R. C.: A high spatial resolution retrieval of NO_2 column densities from OMI: method and evaluation, Atmos. Chem.

Phys., 11, 8543-8554, 2011.

Russell, A. R., Valin, L. C., and Cohen, R. C.: Trends in OMI NO_2 observations over the US: effects of emission control technology and the economic recession, Atmos. Chem. Phys., 12, 12197-12209, 2012.

Souri, A. H., Choi, Y., Jeon, W., Li, X., Pan, S., Diao, L., and Westenbarger, D. A.: Constraining NOx emissions using satellite NO_2 measurements during 2013 DISCOVER-AQ Texas campaign, Atmos. Environ., 131, 371-381, 2016.

Strahan, S. E., Duncan, B. N., and Hoor, P.: Observationally derived transport diagnostics for the lowermost stratosphere and their application to the GMI chemistry and transport model, Atmos. Chem. Phys., 7, 2435-2445, 2007.

Streets, D. G., Canty, T., Carmichael, G. R., de Foy, B., Dickerson, R. R., Duncan, B. N., Edwards, D. P., Haynes, J. A., Henze, D. K., Houyoux, M. R., Jacob, D. J., Krotkov, N. A., Lamsal, L. N., Liu, Y., Lu, Z., Martin, R. V., Pfister, G. G., Pinder R. W., Salawitch, R. J., Wecht, K. J.: Emissions estimation from satellite retrievals: A review of current capability, Atmos. Environ., 77, 1011-1042, 2013.

Strode, S. A., Rodriguez, J. M., Logan, J. A., Cooper, O. R., Witte, J. C., Lamsal, L. N., Damon, M., Van Aartsen, B., Steenrod, S. D., and Strahan, S. E.: Trends and variability in surface ozone over the United States, J. Geophys. Res. Atmos., 120, 9020-9042, 2015.

Travis, K. R., Jacob, D. J., Fisher, J. A., Kim, P. S., Marais, E. A., Zhu, L., Yu, K., Miller, C. C., Yantosca, R. M., and Sulprizio, M. P.: Why do models overestimate surface ozone in the Southeast United States, Atmos. Chem. Phys., 16, 13561-13577, 2016.

Val Martin, M., Honrath, R. E., Owen, R. C., Pfister, G., Fialho, P., and Barata, F.: Significant enhancements of nitrogen oxides, black carbon, and ozone in the North Atlantic lower free troposphere resulting from North American boreal wildfires, J. Geophys. Res. Atmos., 111, 2006.

van Donkelaar, A., Martin, R. V., Leaitch, R. W., Macdonald, A. M., Walker, T. W., Streets, D. G., Zhang, Q., Dunlea, E. J., Jimenez, J. L., and Dibb, J. E.: Analysis of aircraft and satellite measurements from the Intercontinental Chemical Transport Experiment (INTEX-B) to quantify long-range transport of East Asian sulfur to Canada, Atmos. Chem. Phys., 8, 2999-3014, 2008.

van Vuuren, D. P., Bouwman, L. F., Smith, S. J., and Dentener, F.: Global projections for anthropogenic reactive nitrogen emissions to the atmosphere: an assessment of scenarios in the scientific literature, Current Opinion in Environmental Sustainability, 3, 359-369, 2011.

Vandaele, A. C., Hermans, C., Simon, P. C., Carleer, M., Colin, R., Fally, S., Merienne, M.-F., Jenouvrier, A., and Coquart, B.: Measurements of the NO_2 absorption cross-section from 42 000 cm− 1 to 10 000 cm− 1 (238–1000 nm) at 220 K and 294 K, Journal of Quantitative Spectroscopy and Radiative Transfer, 59, 171-184, 1998.

Veefkind, J. P., Aben, I., McMullan, K., Förster, H., De Vries, J., Otter, G., Claas, J., Eskes, H. J., De Haan, J. F., and Kleipool, Q.: TROPOMI on the ESA Sentinel-5 Precursor: A GMES mission for global observations of the atmospheric composition for climate, air quality and ozone layer applications, Remote Sensing of Environment, 120, 70-83, 2012.

Verstraeten, W. W., Neu, J. L., Williams, J. E., Bowman, K. W., Worden, J. R., and Boersma, K. F.: Rapid increases in tropospheric ozone production and export from China, Nat. Geosci., 8, 690, 2015.

Vienneau, D., Hoogh, K. D., Bechle, M. J., Beelen, R., van Donkelaar, A., Martin, R. V., Millet, D. B., Hoek, G., and Marshall, J. D..: Western European land use regression incorporating satellite-and ground-based measurements of NO_2 and PM10, Environ. Sci. & Tech., 47, 13555-13564, 2013.

Vinken, G. C. M., Boersma, K. F., Maasakkers, J. D., Adon, M., and Martin, R. V.: Worldwide biogenic soil NOx emissions inferred from OMI NO_2 observations, Atmos. Chem. Phys., 14, 10363-10381, 2014a.

Vinken, G. C. M., Boersma, K. F., van Donkelaar, A., and Zhang, L.: Constraints on ship NOx emissions in Europe using GEOS-Chem and OMI satellite NO2 observations, Atmos. Chem. Phys., 14, 1353-1369, 2014b.

Young, M. T., Bechle, M. J., and Sampson, P. D., Szpiro, A. A., Marshall, J. D., Sheppard, L., and Kaufman, J. D.: Satellite-Based NO_2 and Model Validation in a National Prediction Model Based on Universal Kriging and Land-Use Regression, Environ. Sci. & Tech., 50, 3686-3694, 2016.

Zhang, L., Jacob, D. J., Boersma, K. F., Jaffe, D. A., Olson, J. R., Bowman, K. W., Worden, J. R., Thompson, A. M., Avery, M. A., Cohen, R. C., Dibb, J. E., Flock, F. M., Fuelberg, H. E., Huey, L. G., McMillan, W. W., Singh, H. B., and Weinheimer, A. J.: Transpacific transport of ozone pollution and the effect of recent Asian emission increases on air quality in North America: an integrated analysis using satellite, aircraft, ozonesonde, and surface observations, Atmos. Chem. Phys., 8, 6117-6136, 2008.

Zoogman, P., Liu, X., Suleiman, R. M., Pennington, W. F., Flittner, D. E., Al-Saadi, J. A., Hilton, B. B., Nicks, D. K., Newchurch, M. J., and Carr, J. L.: Tropospheric emissions: monitoring of pollution (TEMPO), Journal of Quantitative Spectroscopy and Radiative Transfer, 186, 17-39, 2017.

Atmos. Chem. Phys. Discuss., doi:10.5194/acp-2017-219, 2017
Manuscript under review for journal Atmos. Chem. Phys.
Discussion started: 19 April 2017

Atmospheric Chemistry and Physics Discussions

Figures

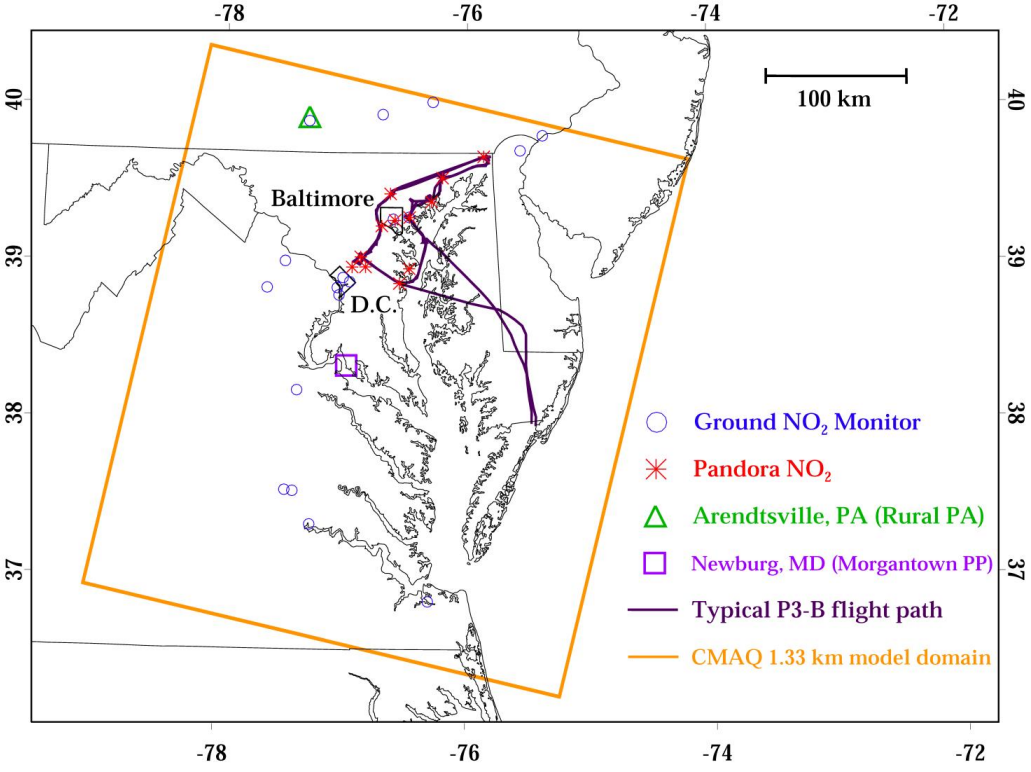

Figure 1. The Mid-Atlantic United States: the area of interest for this research project. Model domain and observation locations are depicted. There are eighteen EPA chemiluminescence monitors and twelve Pandora NO_2 measurement sites.

Atmos. Chem. Phys. Discuss., doi:10.5194/acp-2017-219, 2017
Manuscript under review for journal Atmos. Chem. Phys.
Discussion started: 19 April 2017

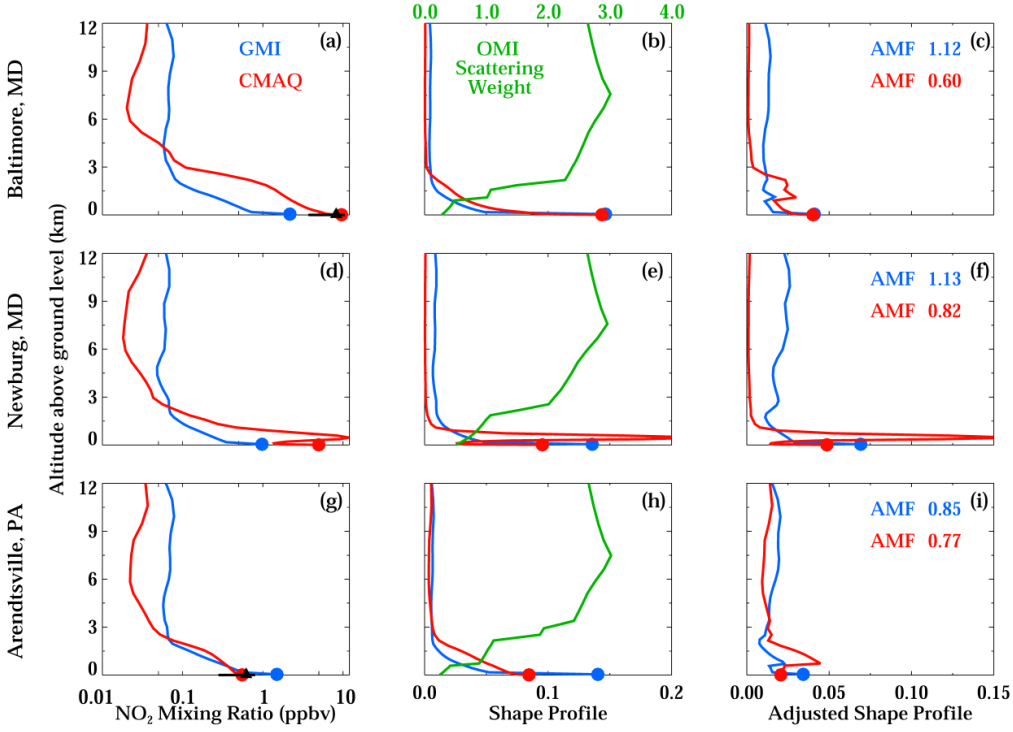

Figure 2. **(a, d, g)** Mean 2 PM local time June and July 2011 NO_2 mixing ratio as a function of altitude from a GMI (1.25° × 1°; ~110 ×110 km) model simulation and CMAQ (1.33 × 1.33 km) model simulation for three locations: **(a)** downtown Baltimore, **(d)** Morgantown power plant in Newburg, MD and **(g)** Arendtsville in rural Pennsylvania. Black triangles with error bars as discussed in the text represent co-located surface observations from the EPA monitoring network. **(b, e, h)** NO_2 shape profiles, partial NO_2 columns divided by total NO_2 column, as function of altitude for the same timeframe and locations; green line denotes co-located OMI scattering weight. **(c, f, i)** "Adjusted" shape profiles, partial NO_2 columns divided by total NO_2 columns multiplied by OMI scattering weight, as function of altitude for the same timeframe and locations.

Atmos. Chem. Phys. Discuss., doi:10.5194/acp-2017-219, 2017
Manuscript under review for journal Atmos. Chem. Phys.
Discussion started: 19 April 2017

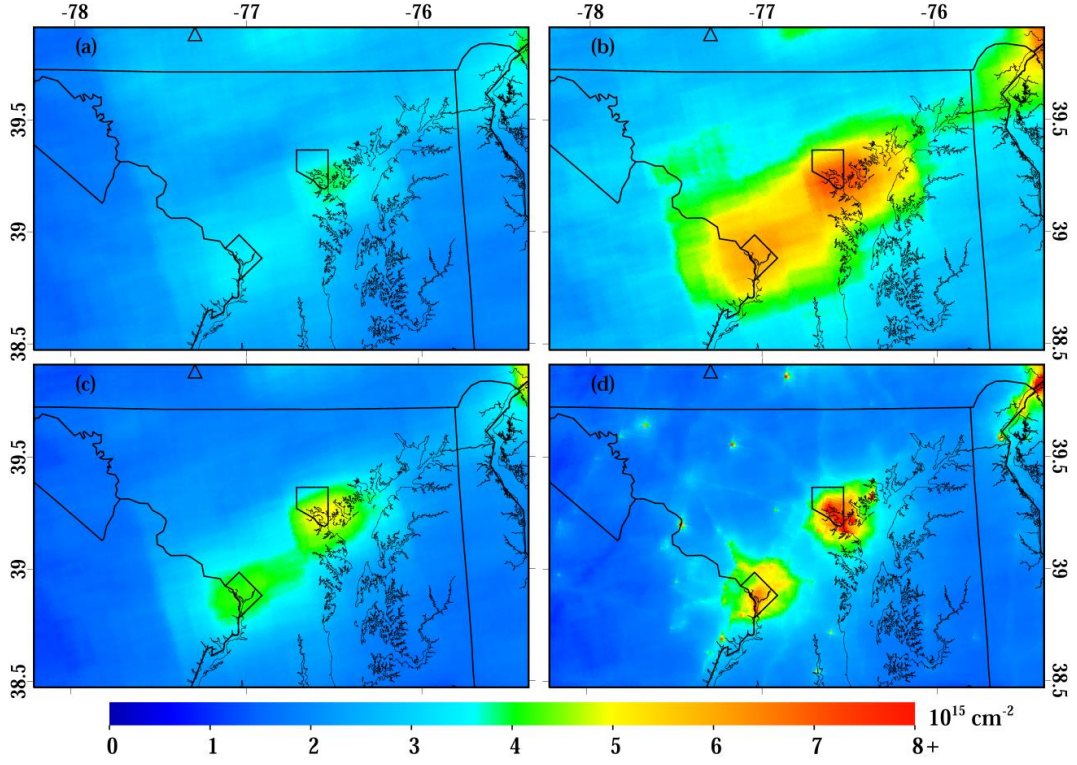

Figure 3. Oversampled OMI NO_2 tropospheric columns at 1.33 km resolution in the Baltimore-Washington metropolitan area for June & July 2008 – 2012 (2 months × 5 years; 10 months total). **(a)** The NASA version 3.0 operational OMI NO_2 product using GMI NO_2 shape profiles (OMI_GMI). **(b)** OMI NO_2 using CMAQ a priori NO_2 shape profiles (OMI_CMAQ). **(c)** OMI NO_2 using CMAQ a priori NO_2 shape profiles constrained by observations (OMI_CMAQ _O). **(d)** OMI NO_2 using CMAQ a priori NO_2 shape profiles constrained by observations and spatial weighting downscaling kernels (OMI_CMAQ_OD). In all plots, Arendtsville, PA is denoted by the triangle.

Atmos. Chem. Phys. Discuss., doi:10.5194/acp-2017-219, 2017
Manuscript under review for journal Atmos. Chem. Phys.
Discussion started: 19 April 2017

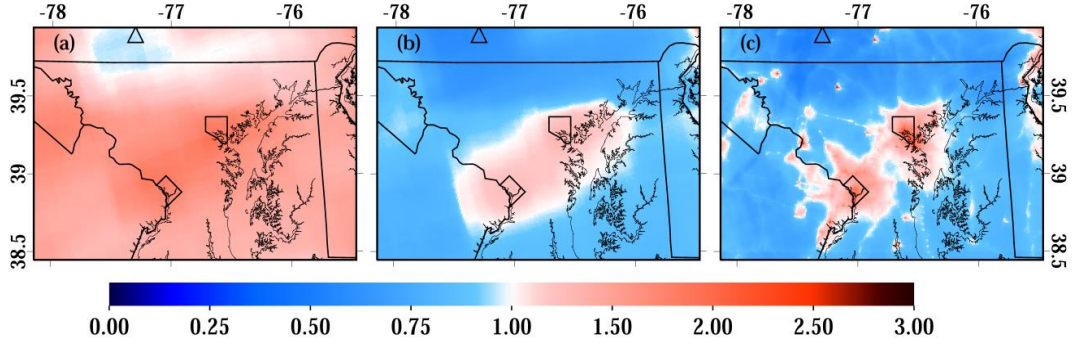

Figure 4. Ratio between the three OMI_CMAQ tropospheric NO_2 retrievals and the operational NASA v3.0 OMI tropospheric NO_2 retrieval for June & July 2008 – 2012 (2 months × 5 years; 10 months total). **(a)** OMI_CMAQ / OMI_GMI. **(b)** OMI_CMAQ_O/ OMI_GMI. **(c)** OMI_CMAQ_OD/ OMI_GMI.

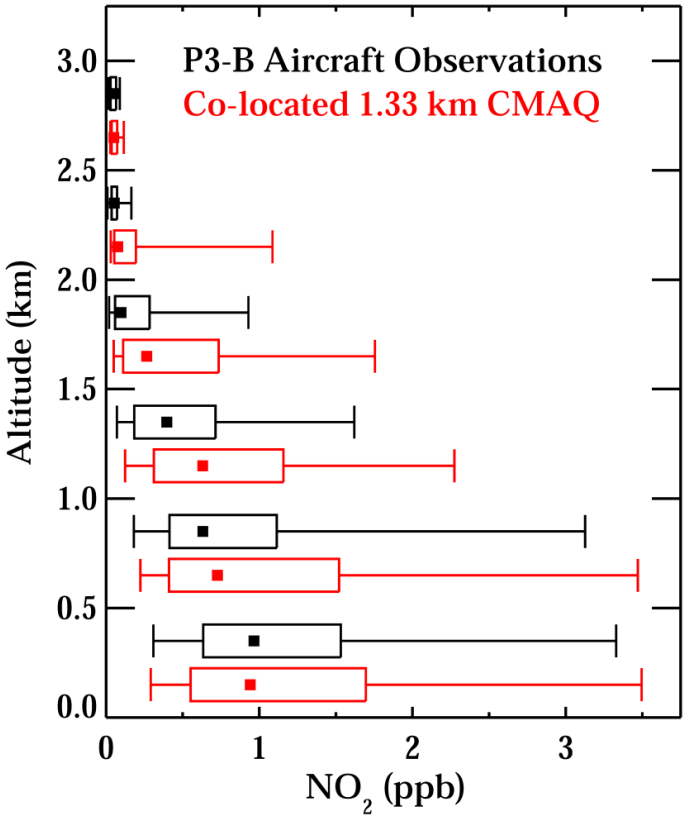

Figure 5. Vertical profiles of NO_2 binned in 500 m intervals (0 – 0.5 km, 0.5 – 1km, etc.) showing the 5th, 25th, 50th, 75th, and 95th percentiles within ± 2 hours of the OMI overpass time. **(Black)** One minute averaged data from the P3-B aircraft during DISCOVER-AQ Maryland. **(Red)** Model output from CMAQ matched spatially and temporally to the P3-B measurements at 1 min intervals. In both cases, the squares indicate the median values.

Atmos. Chem. Phys. Discuss., doi:10.5194/acp-2017-219, 2017
Manuscript under review for journal Atmos. Chem. Phys.
Discussion started: 19 April 2017

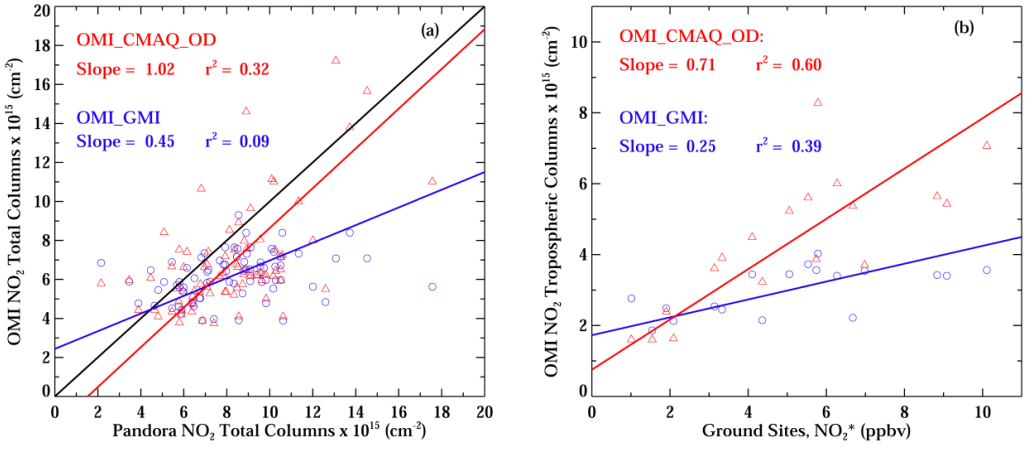

Figure 6. OMI NO_2 column amounts vs. in situ observations. **(a)** Total column NO_2 OMI_GMI and OMI_CMAQ_OD versus co-located spatially and temporally Pandora NO_2 total column measurements within ± 1 hour of a valid satellite overpass during July 2011. **(b)** Tropospheric column NO_2 OMI_GMI and OMI_CMAQ_OD versus co-located ground NO_2* chemiluminescence measurements within ± 2 hours of a valid satellite overpass during June & July 2008 through 2012; all ~300 daily ground monitor values are merged into a mean single value and compared to the satellite mean over the same corresponding time period.

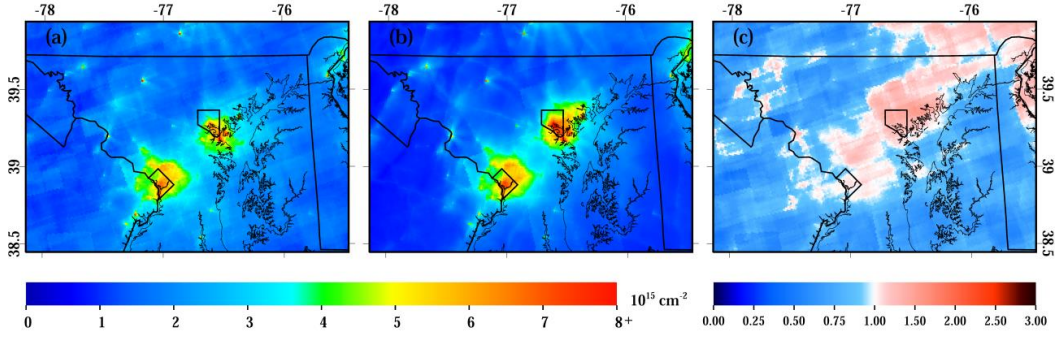

Figure 7. Oversampled tropospheric column NO_2 at 1.33 km in the Baltimore-Washington metropolitan area for June & July 2011 only. **(a)** OMI_CMAQ_OD. **(b)** CMAQ NO_2 corresponding to valid overpass times. **(c)** Ratio between the two plots CMAQ / OMI_CMAQ_OD.

Atmos. Chem. Phys. Discuss., doi:10.5194/acp-2017-219, 2017
Manuscript under review for journal Atmos. Chem. Phys.
Discussion started: 19 April 2017

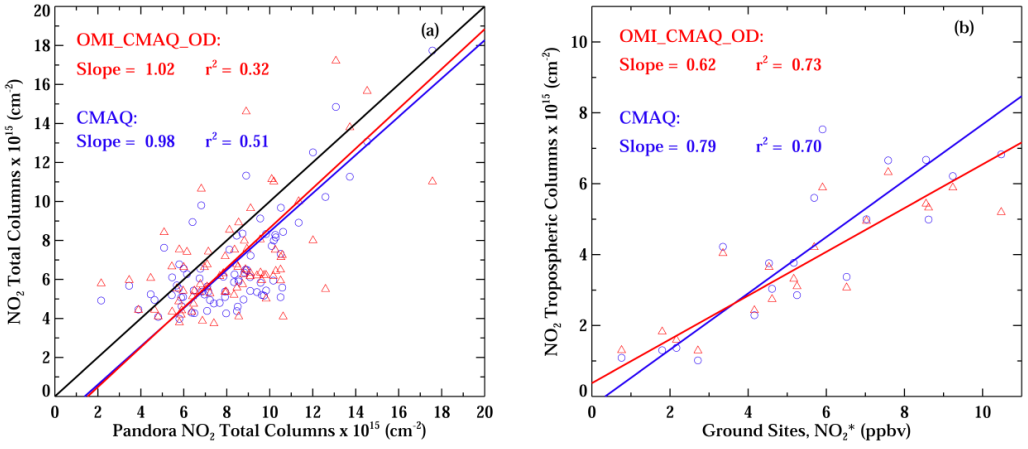

Figure 8. (a,b) Same as Figure 6(a,b), but now showing CMAQ instead of OMI_GMI. **(b)** Showing June & July 2011 only due to model availability during this timeframe.

Table 1. Slope and r^2 for all four OMI satellite products compared to Pandora NO_2 from July 2011 and EPA ground monitor NO_2* observations from June & July 2008 – 2012. Pandora NO_2 is compared to the OMI NO_2 total column products, while the EPA ground monitors are compared to OMI NO_2 tropospheric column products. Figure 6 shows values for OMI_GMI and OMI_CMAQ_OD only.

	Pandora NO_2		EPA NO_2*	
	Slope	r^2	Slope	r^2
OMI_GMI	0.45	0.09	0.25	0.39
OMI_CMAQ	1.27	0.11	0.54	0.55
OMI_CMAQ_O	0.67	0.16	0.41	0.57
OMI_CMAQ_OD	1.02	0.32	0.71	0.60